Cambridge Centre for Computational Chemical Engineering

University of Cambridge

Department of Chemical Engineering

Preprint ISSN 1473 – 4273

A study on the coagulation of polycyclic aromatic hydrocarbon clusters to determine their collision efficiency

Abhijeet Raj [1] Markus Sander [1] Vinod Janardhanan [1] Markus Kraft [1]

released: 01 June 2009

[1] Department of Chemical Engineering
University of Cambridge
New Museums Site
Pembroke Street
Cambridge, CB2 3RA
UK
E-mail: mk306@cam.ac.uk

Preprint No. 73

c4e

Key words and phrases: PAH, soot, aromatic site, dimerisation, kinetic Monte-Carlo, simulation, modelling

Edited by
Cambridge Centre for Computational Chemical Engineering
Department of Chemical Engineering
University of Cambridge
Cambridge CB2 3RA
United Kingdom.

Fax: + 44 (0)1223 334796
E-Mail: c4e@cheng.cam.ac.uk
World Wide Web: http://www.cheng.cam.ac.uk/c4e/

Abstract

This paper presents a theoretical study on the physical interaction between polycyclic aromatic hydrocarbons (PAHs) and their clusters of different sizes in premixed laminar flames. Two models are employed for this study: a detailed PAH growth model, referred to as the kinetic Monte Carlo—aromatic site (KMC-ARS) model [Raj *et al.*, Combust. Flame, 2009]; and a multivariate PAH population balance model, named as the PAH—primary particle (PAH-PP) model. Both the models are solved by kinetic Monte Carlo methods. PAH mass spectra are generated using the PAH-PP model, and compared to the experimentally observed spectra for a premixed laminar ethylene flame. The position of the maxima of PAH dimers in the spectra and their concentrations are found to depend strongly on the collision efficiency of PAHs. The variation in the collision efficiency with various flame and PAH parameters is studied to determine the factors on which it may depend. A correlation for the collision efficiency is proposed by comparing the computed and the observed spectra for an ethylene flame. With this correlation, a good agreement between the computed and the observed spectra for a number of premixed laminar ethylene flames is found.

Contents

1 Introduction

Soot particles, which contribute significantly to the atmospheric nanoparticles, are well known to cause adverse health problems upon inhalation. Some of its consequences can be increase in underlying pulmonary and cardiac problems leading to earlier death or increased morbidity [25]. Apart from the health threats, soot particles are responsible for heat loss in combustion devices through radiation. In contrast, carbon black, which is very similar to soot but with higher surface area to volume ratio, is used in industries as pigments in inks, coatings and plastics, and as reinforcement in rubber and plastic products. In order to reduce or enhance the production of these substances, it is important to gain insight into their formation and growth pathways [21].

In the last few decades, several theoretical and experimental investigations have been conducted in order to understand the mechanism of soot formation. In [6, 22, 39, 40], morphological studies were conducted on soot particles from engines and laboratory flames using High Resolution Transmission Electron Microscopy (HRTEM), X-Ray diffraction techniques and Dark Field Transmission Electron Microscopy (DFTEM). These studies revealed that mature soot particles are microcrystalline near the outer edge and exhibit amorphous nature in the core. This crystallinity arises due to stacking of planar PAHs to form parallel atomic layers and their alignment along the periphery of soot particles. The recent experimental findings of Vander Wal et al. [42] indicate that the amorphous nature of soot nuclei or core is due to the presence of randomly oriented and/or non-planar PAHs. It is clear from these studies that PAH molecules act as a soot precursor, and their relative orientations decide the graphitic or amorphous nature of soot particles. In [1, 41], the variations in the structure of the PAHs, their sizes and their orientations in soot particles generated from different fuels under different physical conditions were studied. Such PAH characteristics were found to depend heavily on the type of the fuel producing it, fuel flow rate and the temperature. For most of the fuel mixtures investigated in their work, nascent soot particles present at low temperatures were amorphous in nature. At higher temperatures, the formation of parallel stacks of PAHs near the outer edge was observed, which are energetically more favoured. It was postulated in [41] that the potential energy barrier required for the re-orientation of the PAHs in soot particles were overcome at high temperatures, and therefore, graphitisation of soot particles took place. For very high fuel flow rates and at high temperatures, curved PAHs were also observed in soot particles. From the above findings, it can be concluded that the characteristics of the PAHs comprising soot depend strongly on the combustion environment, in which they are produced. Therefore, to study the soot formation process in a given environment, the knowledge about the evolving structures of PAHs in it is essential.

To facilitate the study of growth of PAH molecules in a combustion environment, a detailed PAH chemical mechanism is available in the literature based on the abundant gaseous species such as C_2H_2, H and small aromatic compounds such as benzene and naphthalene [13, 44, 45]. Recently, a number of models have been proposed to study PAH growth in flame environments [15, 32, 43]. The PAH growth model presented by Violi [43] models large, non-planar PAH sheets in a flame-like environment. A large set of reactions describe the growth of a PAH molecule, using a kinetic Monte Carlo (KMC) algorithm. Molecular dynamics (MD) calculations [43] are used to optimise the PAH

geometry. An another PAH model is proposed in [32], in which a single planar PAH molecule is simulated using a kinetic Monte Carlo algorithm. It is shown through the KMC simulations that the present reaction mechanism predicts, reasonably well, the ensembles of PAHs observed in different flame environments. Such models provide a useful tool to study the surface growth of PAHs or soot particles.

Along with the surface reactions, a physical process, that can take place simultaneously, is the coagulation of PAHs. The presence of PAH stacks and clusters in the experimental HRTEM images of soot particles, as discussed above, indicates that the coagulation of PAHs may be responsible for soot nucleation. This hypothesis has provoked a large number of theoretical studies on the stability and relative orientation of PAHs present in dimers and higher order stacks (such as trimers) in flame environments [20, 26–29, 34, 35]. In soot models, pyrene dimerisation is considered to be the soot nucleation step (the transition from gaseous molecules to soot particles) [4, 37]. The validity of this assumption has been tested in a number of studies [3, 35], and is still debated [18]. In one of the earlier studies on PAH coagulation [29], the equilibrium constant for this process, $\mathrm{A} + \mathrm{B} \rightleftharpoons \mathrm{AB}$ was determined by assuming that all steps are reversible and that equilibrium is attained at each step. Using the calculated equilibrium constants, the concentration of PAH dimers was evaluated, and it was concluded that the PAH dimerisation may not be responsible for soot nucleation, as the number density for newly incepted soot particles in flames were severely under-predicted. In [12], the authors argued that the assumption of equilibrium after PAH coagulation may not hold in a flame environment, and the dimerisation process may proceed irreversibly. The PAH coagulation flux needs to be computed kinetically instead of using the equilibrium assumption. In [19], the concentration profiles of PAHs present in aliphatic flames were observed experimentally. This study concluded that it is possible to predict the number density of incepted soot particles by taking into account the coagulation of PAHs. This result did not agree with the findings of Miller *et al.* [29] due to the very low concentration of PAHs assumed in their study to calculate the number density. To determine the contribution of PAHs and $\mathrm{C_2H_2}$ in soot nucleation and growth, another study was conducted by Mckinnon *et al.* [26]. In their study, it was found that, to predict the soot volume fraction observed in a sooting benzene flame, a PAH collision efficiency of 0.1 to 0.5 was required (collision efficiency is the probability of coagulation after collision, and is a factor multiplied to the gas kinetic rate for PAH collision in a given pressure regime to obtain an estimate of the PAH coagulation rate [36].). A similar range was proposed by Miller in a kinetic study on PAH agglomeration [27]. Recently, the value of coagulation efficiency for small nanoparticles has been determined experimentally by D'Alessio *et al.* [7]. For particles below 2 nm, this value has been proposed to be less than 0.01. To model the soot nucleation and/or PAH coagulation process, different collision efficiencies have been used in the literature: 1 in [12], 0.3 in [9], and between 10^{-5} and 1 in [8]. In [8], a soot model was presented to take into account simultaneous formation and growth of particulates and PAH molecules using a sectional method. The authors concluded in this study that the PAH coagulation processes in their reaction mechanism did not play a vital role due to low values of coagulation efficiencies assumed for the PAHs larger than pyrene. It was shown that a significant variation in the predicted particulate volume fraction can be obtained with the change in collision efficiency, and thus, is an important factor for the theoretical study of soot nucleation. Based on the above arguments, in the present work, detailed analyses on the variation of collision efficiency with flame

temperature and PAH characteristics have been conducted.

This paper attempts to lay the foundation for a soot model based entirely on the formation, growth and coagulation of PAHs and their clusters of different sizes using kinetic Monte Carlo methods. Such a soot model will be presented, and used to conduct a theoretical study on the interaction between PAHs. The PAH ensembles required for this study will be generated computationally at different heights above the burner (HABs) in premixed laminar ethylene flames using the previously proposed PAH growth model (the KMC-ARS model) and an extended PAH growth mechanism. The PAH mass spectra will be generated computationally to determine the relative abundance of PAH clusters in the ensemble, and compared to the experimentally observed mass spectra for several premixed laminar flames.

2 KMC-ARS model

A detailed PAH growth model, named as the KMC-ARS model, has been employed previously to study the growth of a single PAH molecule in different flame environments [5, 32, 33]. The main features of the model are summarised here. The KMC-ARS model describes a PAH molecule in terms of the number of reactive sites present along its outer edge. Figure 1 shows an example PAH molecule with different types of sites [32]: free-edges, zig-zags, armchairs, bays, and five-member rings. This model utilises a kinetic

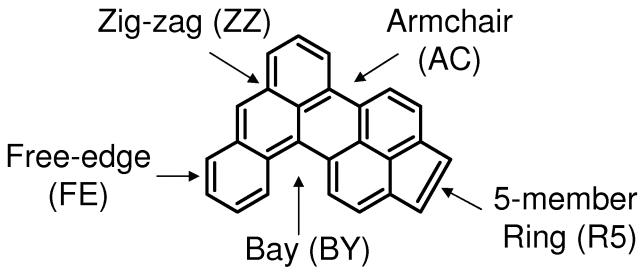

Figure 1: *An example PAH showing the principal surface site types, which are involved in the surface reactions.*

Monte Carlo algorithm along with a detailed reaction mechanism to simulate the growth of a PAH molecule. The reaction mechanism used previously [32] has been extended in this work by including the new PAH reactions proposed in [33]. With this model, it is possible to track the planar structure of the PAHs as it grows in a chemical environment. This is done by tracking the positions of the C atoms, and the information about the reactive sites, of which each surface C atom is a part. The structural assumption of the planar growth of PAHs in this model makes it computationally much faster than the PAH growth models employing KMC algorithm with molecular dynamics [43].

The computational study of soot inception or PAH coagulation requires the simultaneous simulation of a large number of PAHs, in which, along with their surface growth, the PAHs are also allowed to coagulate together to form clusters. With the KMC-ARS model,

it becomes computationally very expensive to simultaneously simulate the surface growth and the coagulation of numerous PAHs. This is because, a large amount of structural information is required to be stored for all the PAHs in each simulation run. Therefore, in this work, for the first time, the KMC-ARS model has been combined to a PAH population balance model, which can be used to study the coagulation of PAHs computed using the KMC-ARS model at different residence times. This approach is based on the separation of the two processes, surface growth and coagulation. Two assumptions are made: (a) the rates of the surface growth processes on a PAH are independent of the number of PAHs present in a stack. For example, the rate of armchair growth reaction in a stack, as shown in figure 2, is assumed to be same as the rate of this reaction on an independent PAH ($\mathrm{Phenanthrene} + \mathrm{C_2H_2} \rightarrow \mathrm{Pyrene} + \mathrm{H_2}$). (b) all the reactive sites present on a PAH are equally accessible irrespective of its position or orientation in a PAH stack or cluster. Note that a PAH stack refers to a set of PAHs aligned parallel to each other, and a cluster represents a set of randomly oriented PAHs. If a PAH is present in the core of a soot particle, the reactive sites on it may not be readily accessible to the chemical species such as $\mathrm{C_2H_2}$ and H. Therefore, this assumption on the accessibility of sites may lead to an over-prediction of the soot mass due to over-predicted soot surface growth rate. However, such information about the accessibility of a site on a PAH in a soot particle is not available. Therefore, the surface growth on PAHs were simulated by uniformly selecting a site present on a PAH.

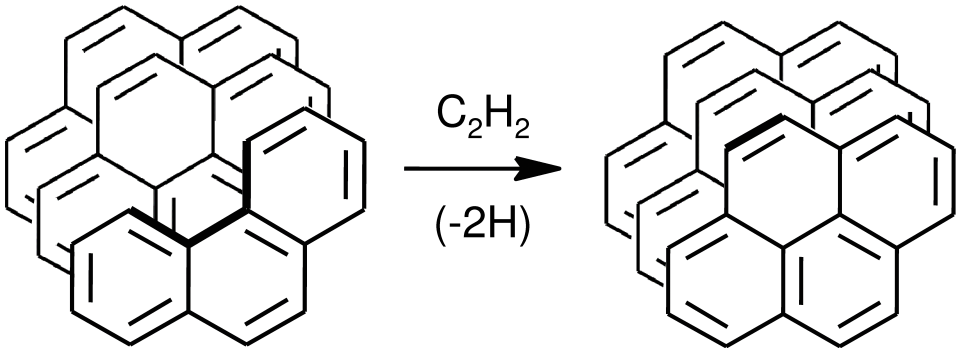

Figure 2: *Armchair growth reaction on a PAH present in a stack. The model assumes that the rate of a reaction on a PAH is independent of the number of PAHs present in a stack.*

With the above assumptions, PAH ensembles were generated in different flame environments, using the algorithm described in [32]. The following section provides the information about the premixed laminar ethylene flames, which were selected for this work.

3 Flame simulation

Table 1 lists the premixed laminar flames simulated in this work to study the growth of PAHs and the formation of their clusters such as dimers and trimers.

Table 1: *Flame initial conditions [16].*

Flame	Pressure (mbar)	Fuel	Composition (mole %)		Cold gas velocity (cm/s)	Mass flux $\times 10^3$ (g/s.cm^2)
			Fuel	O_2		
1	80	C_2H_4	50	50	54	5.37
2	120	C_2H_4	50	50	54	8.05
3	150	C_2H_4	50	50	54	10.07
4	180	C_2H_4	50	50	54	12.08
5	220	C_2H_4	50	50	54	14.76

The reason behind choosing these flames was the availability of the experimentally observed mass spectra of PAH monomers and dimers. The species concentration and the temperature profiles for these flames were not measured. This information was obtained by simulating the flames using the ABF chemical mechanism [2] along with the CHEMKIN package [24] and PREMIX [23]. The ABF chemical mechanism has been validated previously by comparing the experimental species profiles with the computed ones for a number of premixed laminar aliphatic flames [2, 32]. Figure 3 shows the computed species and temperature profiles for the flames 1–5. With these simulated profiles, the PAH growth simulation was carried out using the KMC-ARS model. Pyrene was taken as the starting structure or the seed molecule for all the simulations. For each flame environment, growth of 1000 PAH molecules were simulated. The information about the composition of all the PAHs (number of C and H atoms) at different residence times (or heights above the burner, HABs) in flames were stored. This information will be referred to as PAH trajectories in flames from now onwards. Figure 4 shows the PAH number distribution in the ensemble of PAHs at different heights above the burner for flames 1–5. With increasing pressure, an increase in the number of large PAH molecules was observed. At HAB = 0 mm, only pyrene was present, as it was chosen as the seed molecule. At lower HABs ($\leq$ 10 mm), PAHs with less than 150 C atoms were present in abundance. However, at higher HABs, the PAH ensembles were mostly dominated by the PAHs having C atom count in the range of 16–500. To study the coagulation of these computed PAHs, a stochastic population balance model was required, and is briefly detailed in the next section.

4 PAH—primary particle (PAH-PP) model

A multivariate PAH population balance model, named as the PAH-PP model, is developed to study the coagulation of PAHs. A kinetic Monte Carlo algorithm is employed to solve the model. It is assumed that the PAH growth processes are independent of the particle structure as a consequence of the assumptions made in the KMC-ARS model. The outcome of this coagulation model depends on the concentrations of the colliding PAHs, their probability of a successful collision (collision efficiency) and the frequency of PAH collision. For the two colliding PAHs a and b, the rate of coagulation $R_{C_{a,b}}$ is given by the

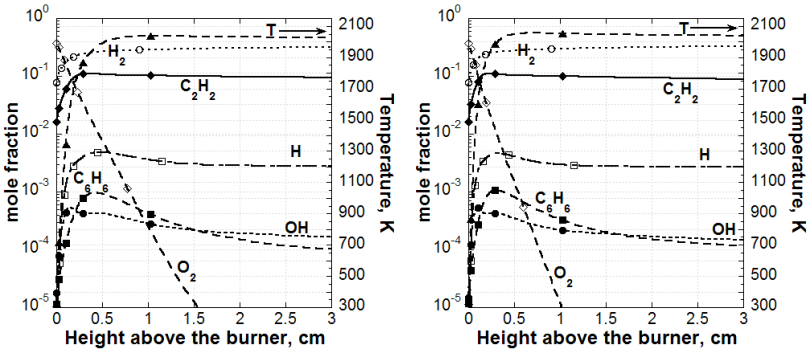

(a) Flame 1

(b) Flame 2

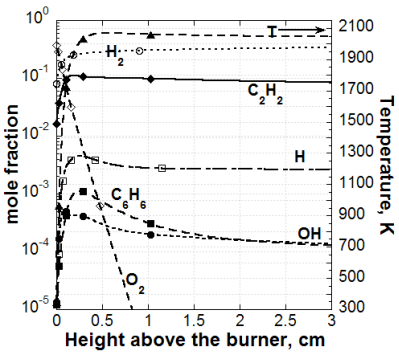

(c) Flame 3

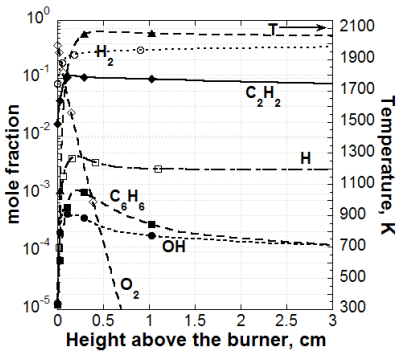

(d) Flame 4

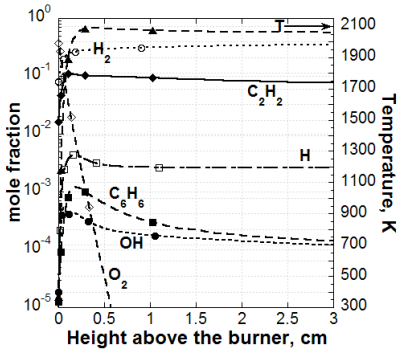

(e) Flame 5

Figure 3: *Computed profiles of the major chemical species present in flames 1–5 at height above the burner (HAB) = 30 mm. These profiles were used to study the growth of PAHs in the flame environments.*

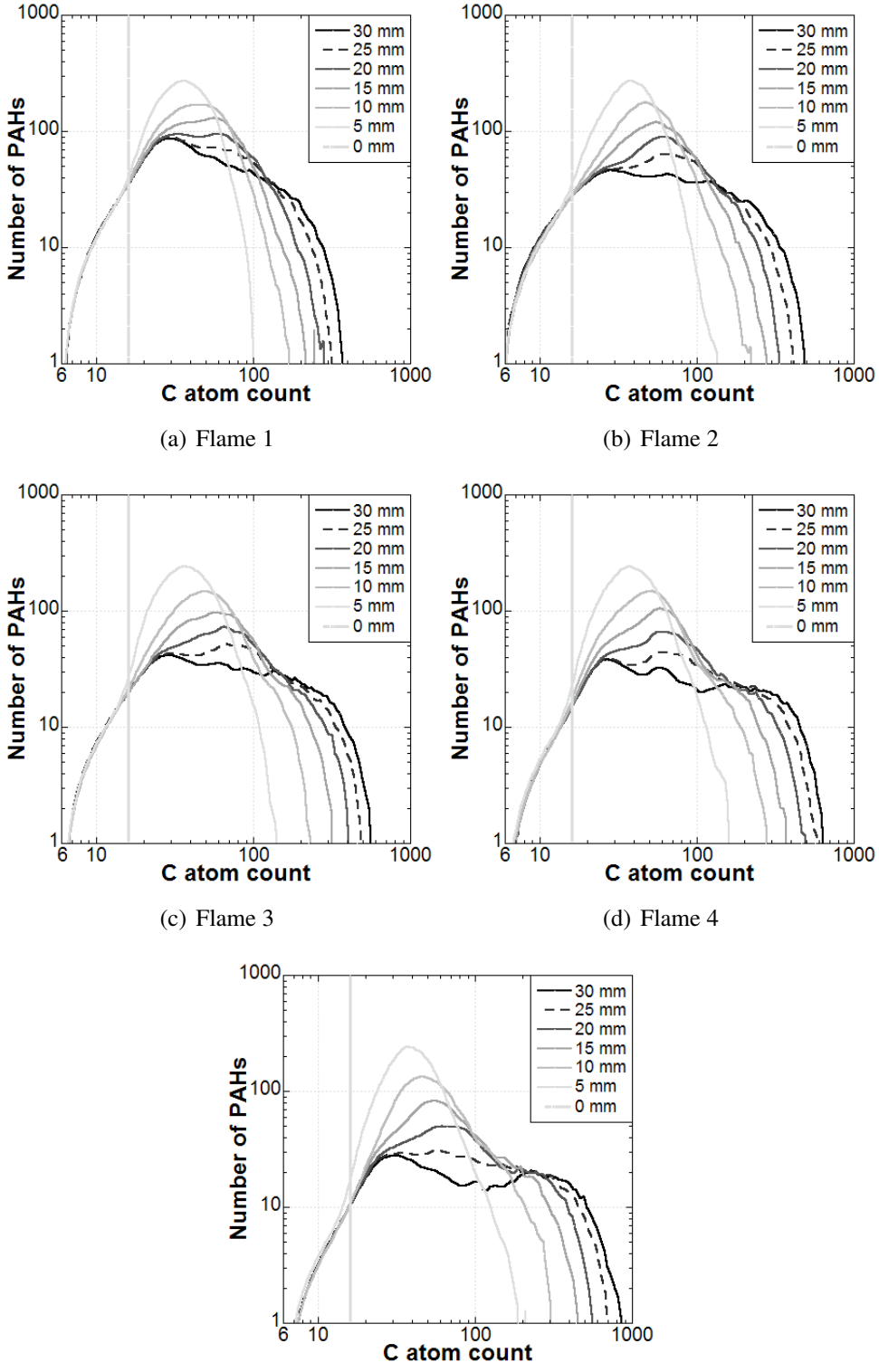

(a) Flame 1

(b) Flame 2

(c) Flame 3

(d) Flame 4

(e) Flame 5

Figure 4: *Variation in the number of PAHs with C atom count (mass distribution) in an ensemble containing 1000 PAH molecules at different HABs for flames 1–5.*

following expression:

$$R_{C_{a,b}} = C_E \times E_F \times \beta_{a,b} \times C_a \times C_b \tag{1}$$

where, C_E is the collision efficiency, $E_F(= 2.2)$ is the van der Waals enhancement factor [19], $\beta_{a,b}$ is the coagulation kernel [36] (a measure of the frequency of PAH collisions), and C_a and C_b are the concentrations of colliding PAHs a and b, respectively. For this work, the expression for $\beta_{a,b}$ in a free molecular regime was used, which is given as [14]:

$$\beta_{a,b} = \sqrt{\frac{\pi k_B T}{2\mu_{a,b}}} \times (2D_{avg})^2$$

where, k_B is the Boltzmann constant, T is the flame temperature, and D_{avg} is the average collision diameter of the colliding PAHs. The collision diameter of a PAH monomer, D_{PAH} can be evaluated using the following expression for peri-condensed PAHs [14]:

$$D_{PAH} = d_A \sqrt{\frac{2 \times n_C}{3}}$$

where d_A denotes the size of a single aromatic ring and equals $1.395\sqrt{3}$ Å, and n_{C} is the number of C atoms in the PAH. For the PAH clusters with n_{PAH} number of PAHs, the collision diameter, D_{col} is evaluated in the following way:

$$D_{col} = \max(D_{\mathrm{PAH}}^{\mathrm{max}},\ D_{\mathrm{sphere}}) \tag{2}$$

where $D_{\mathrm{PAH}}^{\mathrm{max}}$ is the collision diameter of the biggest PAH in the cluster, and D_{sphere} is the collision diameter of a spherical particle with the mass PAH cluster and the density of $1.8\,\mathrm{g/cm^3}$ (same as soot density). For small PAH clusters, $D_{\mathrm{PAH}}^{\mathrm{max}}$ is larger than D_{sphere}, and vice-versa for large clusters.

At time t, an exponentially distributed waiting time for the coagulation process to take place, τ with parameter λ is calculated, where λ is the sum of the rates of all possible coagulation events in an ensemble having $n(t)$ number of PAH clusters [14, 36]:

$$\lambda = \frac{1}{2} \sum_{i=1}^{n(t)} \sum_{j=1}^{n(t)} R_{C_{i,j}}$$

The time for the next process is calculated as $t = t + \tau$. Two PAH clusters are chosen from the ensemble for coagulation based on a probability calculated using their coagulation rate. In order to computationally fasten the above steps, an stochastic algorithm for coagulation, provided in [10, 30], was employed. After each coagulation event, the information about all the PAHs present in the ensemble was updated based on the database of PAH trajectories. The whole procedure was repeated for the desired simulation time.

In order to follow the above procedure, the model requires a multi-dimensional data structure to store various information about each PAH cluster present in the ensemble such as number of PAHs in the cluster, their mass and diameter, and a unique identifier for each PAH molecule. The further details about this model, and its predictive capability of soot observables such as soot volume fraction, particle diameters and particle size distribution functions in flames will be detailed in a forthcoming publication.

5 Results and discussion

A PAH mass spectra is required to obtain information about the abundance of different PAHs present in a flame. Recently, experimental studies have been conducted on a number of premixed laminar flames to obtain the PAH mass spectra using photoionisation mass spectroscopy [16–18]. The experimental details are briefly reviewed here. The PAH molecules were drawn from the flames via a nozzle, and were diluted in a fast flow reactor. The reactor was connected to a time of flight–mass spectrometer (TOF-MS) via a molecular beam inlet. The TOF-MS was equipped with an excimer laser as a photoionisation source (laser gas ArF or KrF). It was observed in [18] that, with the use of an ArF laser beam, at least 2 photons were required for PAH monomers, and one photon was required for higher order PAH stacks (such as dimers and trimers) for ionisation. Through this study, for the first time, it was possible to obtain the mass spectra for the potential soot precursors, PAH stacks, which may help in understanding the soot formation mechanism. In this work, such spectra of PAH clusters in the premixed laminar flames listed in table 1 were computationally generated using the PAH-PP model. The following sections present the comparison between the experimentally observed and the computed PAH mass spectra.

5.1 PAH mass spectra

In order to calculate the coagulation rate, a value of collision efficiency (C_E) is required (see equation 1). In the first instance, the suggested values of C_E for PAHs in the literature, for example, 0.1–0.5 in [26] and 10^{-5}–1 in [8], were used to simulate the coagulation of PAHs in the environment of flame 2. Figure 5 shows the computed PAH mass spectra for flame 2 when $C_E = 0.3$, an average value of the range (0.1–0.5) suggested in [26]. For comparing the computed and the observed mass spectra, three features were selected: (a) position of the maxima of PAH dimers in the two mass spectra; (b) position in the spectra after which no significant amount of monomers were present; (c) spread of the dimer mass spectra on the either side of the maxima. In the experimental spectra, the concentrations of the PAHs were represented in terms of the intensity of ion signals for different PAH masses [18], whereas, PAH number density was used for the computed spectra. Therefore, the PAH concentrations (specifically, for PAH dimers) can only be compared qualitatively. For the case shown in figure 5, due to a very high value of collision efficiency, negligible amount of PAHs remained as monomers and dimers in the computed ensemble at HAB = 30 mm. Moreover, the computed dimer spectra were found to be widely distributed over a vast PAH mass range of 500 u – 4000 u (not shown here), as compared to the experimentally observed spectra (600 u – 2000 u). Thereafter, C_E was varied between 10^{-5}–1 as a function of the diameters of colliding PAHs [8]. As observed in [8], the suggested variation in C_E led to very few PAH collisions, resulting in a significantly low number density for PAH dimers. These findings clearly indicate that the suggested values for C_E cannot reproduce through simulations, the position of the maxima and the concentration of PAH dimers in the computed spectra. Therefore, in this work, a fitting procedure was adopted to obtain an expression for the collision efficiency, and is detailed in the next section. It should be noted that all the comparisons between experimental

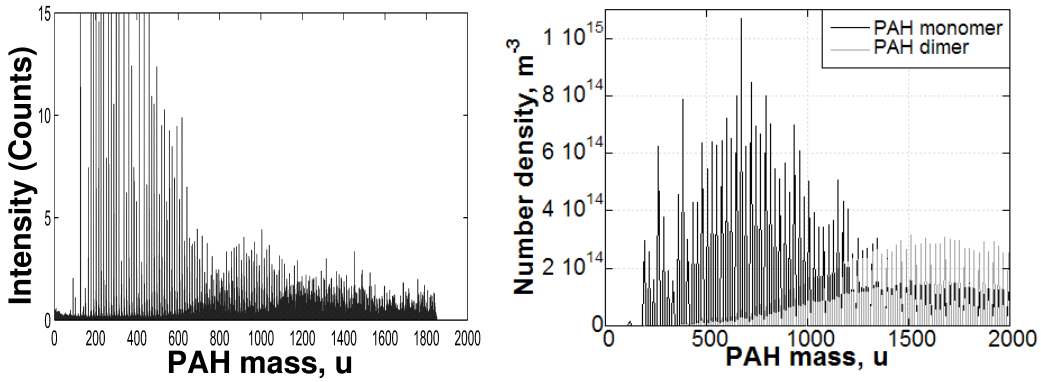

(a) Experimental mass spectra (b) Computed mass spectra

Figure 5: *PAH mass spectra at an operating pressure of 120 mbar (flame 2) at HAB = 30 mm with a constant collision efficiency of 0.3. PAH monomers are represented by black lines, and dimers by grey lines in the computed spectra. Negligible amount of PAH monomers and dimers were present in the PAH ensemble at HAB = 30 mm for such a high value of collision efficiency, as they were consumed in the formation of larger PAH clusters.*

mass spectra and computed spectra shown in this paper are limited to PAH monomers and dimers, as the experimental spectra for higher order PAH stacks were not available for these flames. However, no limitation on the maximum number of PAHs, that can be present in a cluster, was imposed in the simulations.

5.1.1 Collision efficiency

In order to study the variation in collision efficiency, the knowledge about the flame and PAH parameters, which can significantly affect the probability of coagulation after collision, was required. In the literature, a number of theoretical studies have been conducted on PAH dimerisation. These studies were helpful in determining the parameters on which the collision efficiency may depend. For example, in [28] it is mentioned that during the PAH growth process, at some point, the van der Waals attractive potentials can become sufficiently large to hold the PAHs together in the flame environments. Therefore, the size (mass) of the PAHs is an important factor in determining its stability. The soot model developed in [8] considered the successful PAH collisions to depend on the diameters of the colliding PAHs. In [17], the PAH mass spectra in different flame environments were observed, and it was concluded that the flame temperature may play a significant role in successful PAH collisions. A recent study by Herdman *et al.* [20] on PAH clusters shows that their binding energies correlate very well with the reduced mass of the colliding PAHs. The above findings suggest that the collision efficiency may depend on the flame temperature, PAH diameter and/or the PAH mass. In this study, these three parameters were individually tested to determine the ones that highly affect the collision efficiency and provide the desired variation in it, as described below.

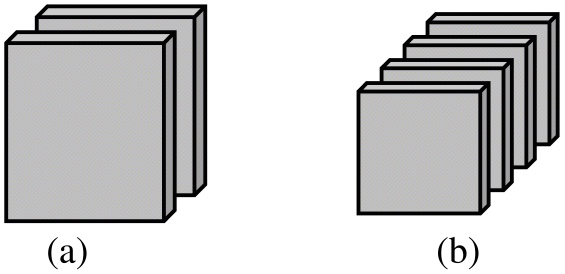

Figure 6: *Two PAH (cuboid) stacks (a and b) with the same mass but different collision diameters and number of constituent PAHs.*

Firstly, the collision efficiency was varied with the flame temperature. At low temperatures (low HABs), only small PAHs were present in the flames in high concentrations. Therefore, collision efficiency close to zero was required to prevent their coagulation in order to avoid the depletion of such PAHs from the ensemble (in other words, to avoid the situation encountered in figure 5). At high temperatures, PAHs of very different sizes were present, and therefore, assuming the same collision efficiency for all such PAHs led to the spreading of dimer spectra over a vast mass range, which is not observed experimentally. Further discussion on the variation of collision efficiency with temperature is provided later in this paper.

Thereafter, the variation in collision efficiency with the average diameter of the colliding PAHs was studied. This variation led to the formation of PAH dimers having a large size difference in the constituent PAHs (for example, a benzene-coronene dimer) due to very high concentrations of small PAHs. The mass spectra produced through simulation for this case predicted the maxima of the PAH dimers at lower PAH masses, and was not consistent with the experimental results. This result suggests that the dimers of PAHs with large size difference (specifically if one of the constituent PAHs is smaller than pyrene) may not be stable in flame environments. This is also hinted at in the study by Miller *et al.* [29], where very low values of equilibrium constant were obtained for the formation of PAH dimers with a large size difference in the constituent PAHs. A similar conclusion was reached in a recent theoretical study on the stability of hetero-molecular PAH dimers in high temperature environments through their binding energy calculations [20].

To reduce the formation of such PAH stacks in the simulation, collision efficiency was varied with the reduced mass of the colliding PAHs, so that a large difference in the masses of the colliding PAHs would produce a low reduced mass, and thus a low value of collision efficiency would be used for the rate calculation. This parameter did not differentiate between the PAH clusters with the same mass, but with different collision diameters and number of PAHs in the cluster, as shown in figure 6. The variation in collision efficiency with reduced mass led to formation of distinguishable humps for PAH monomers and dimers in the computed mass spectra. However, the spectra for dimers were more widely distributed over higher PAH masses than observed experimentally.

From the above observations, two main conclusions were drawn: (a) collision efficiency depends both on the mass as well as on the collision diameter of the colliding PAH clusters, so that the clusters as shown in figure 6 can be differentiated; (b) a successful co-

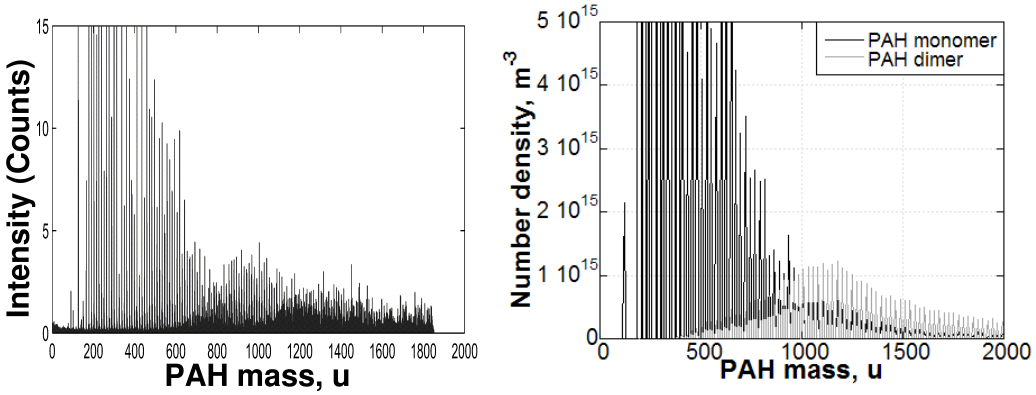

(a) Experimental mass spectra (b) Computed mass spectra

Figure 7: *PAH mass spectra at an operating pressure of 120 mbar (flame 2) at HAB = 30 mm. PAH monomers are represented by black lines, and dimers by grey lines in the computed spectra. The position of the maxima of PAH dimers and the spread of the spectra for dimers on the either side of the maxima were well predicted.*

agulation depends mainly on the mass M_{min} and diameter D_{min} of the smaller of the two colliding clusters. With these two variables for the collision efficiency, an expression of the form, shown in equation 2, was adopted, which could restrict the value of C_E in between 0 and 1 in a desired way.

$$C_E = \frac{1}{1 + \exp\left(-A \times \left(\frac{D_{min}^3}{M_{min}} + \left(\frac{M_{min}}{B}\right)^6 - C\right)\right)} \tag{3}$$

A, B and C in the expression for collision efficiency were obtained by comparing the computed spectra for flame 2 with the experimental spectra. For comparison, the features of the mass spectra, listed in section 5.1 were selected. The parameter values of $A = 2$, $B = 1100$, and $C = 5$ were able to satisfactorily reproduce the experimental spectra for flame 2, as shown in figure 7. Figure 8 shows the range of values for the collision efficiency required for a satisfactory agreement between the computed and the observed spectra for this flame. This figure shows that the collision between two PAH clusters would always lead to coagulation if the smaller PAH cluster has mass and collision diameter, greater than 1200 u and 20 Å, respectively, as C_{E} = 1 for all such clusters. Figure 9 presents a contour plot of collision efficiency. The positions of some of the commonly observed PAHs are marked in this figure. In the simulation, considerable amount of coagulation took place when the mass and collision diameter of the smaller of the two colliding PAHs were greater than 360 u and 10 Å, respectively. An example PAH monomer ($\mathrm{C_{30}H_{14}}$) satisfying such criteria (mass = 374 u, diameter = 10.8 Å) is shown in the figure. The dashed line in the figure represents the line for peri-condensed PAHs such as pyrene, coronene and circumcoronene. The area above this line in the figure is only accessible to PAH clusters with more than one constituent PAHs (for example, a $\mathrm{C_{38}H_{16}}$ dimer).

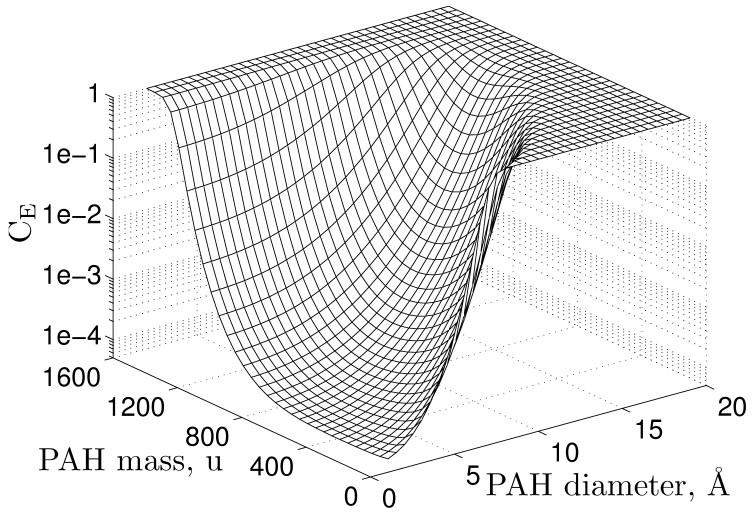

Figure 8: *PAH collision efficiency C_{E} as function of the mass M_{min} and the collision diameter D_{min} of the smaller of the two colliding PAH clusters. C_{E} = 1 if the smaller PAH cluster has mass and collision diameter, greater than 1200 u and 20 Å, respectively.*

The correlation for C_E with the set of parameters obtained for flame 2 was then used to compute the spectra for the flames at different pressures (table 1), and their comparison with the observed spectra is shown in figures 10–13. Figure 14 shows the constituent PAHs of a computed PAH dimer with a mass of 1090 u present in flame 2.

Figure 15 shows the variation in the number fraction of the PAH clusters with the number of PAHs present in the cluster. For a PAH cluster with i number of PAHs, the number fraction, $x_{C,i}$ was calculated using the following expression: $x_{C,i} = N_{C,i} / \sum_{i=1}^{\infty} N_{C,i}$, where $N_{C,i}$ represents the number of clusters in the ensemble with i PAHs. It can be observed in the figure that an increase in pressure increases the number of PAH clusters with large number of PAHs (≥ 40) in them. This is due to the increase in the number of collisions taking place between the PAHs, and the presence of larger PAHs at higher pressures. Interestingly, the increase in pressure changes the unimodal distribution of cluster number fraction to bimodal, which is a typical characteristic of particle size distribution functions (PSDFs). For bimodal PSDFs, the first mode represents nascent or newly incepted soot particles, and the second mode represents the particles formed through coagulation [38]. At 220 mbar, a minimum value for the first mode is observed for clusters with around 10 PAHs in it. Taking the analogy from PSDFs, the PAH clusters with ≤ 10 PAHs may be regarded as nascent soot, and all the higher order PAH clusters, as mature soot particles. This information will be used in a forthcoming publication to study the composition of nascent and mature soot particles in premixed laminar flames, which were experimentally observed in [1].

With the use of proposed correlation for C_E, the computed spectra were able to predict certain trends followed by the experimental spectra. Firstly, the number density of PAH dimers was observed to decrease with increase in pressure. The reason behind this was an increase in the number of PAH collisions with increasing pressure, which led to the

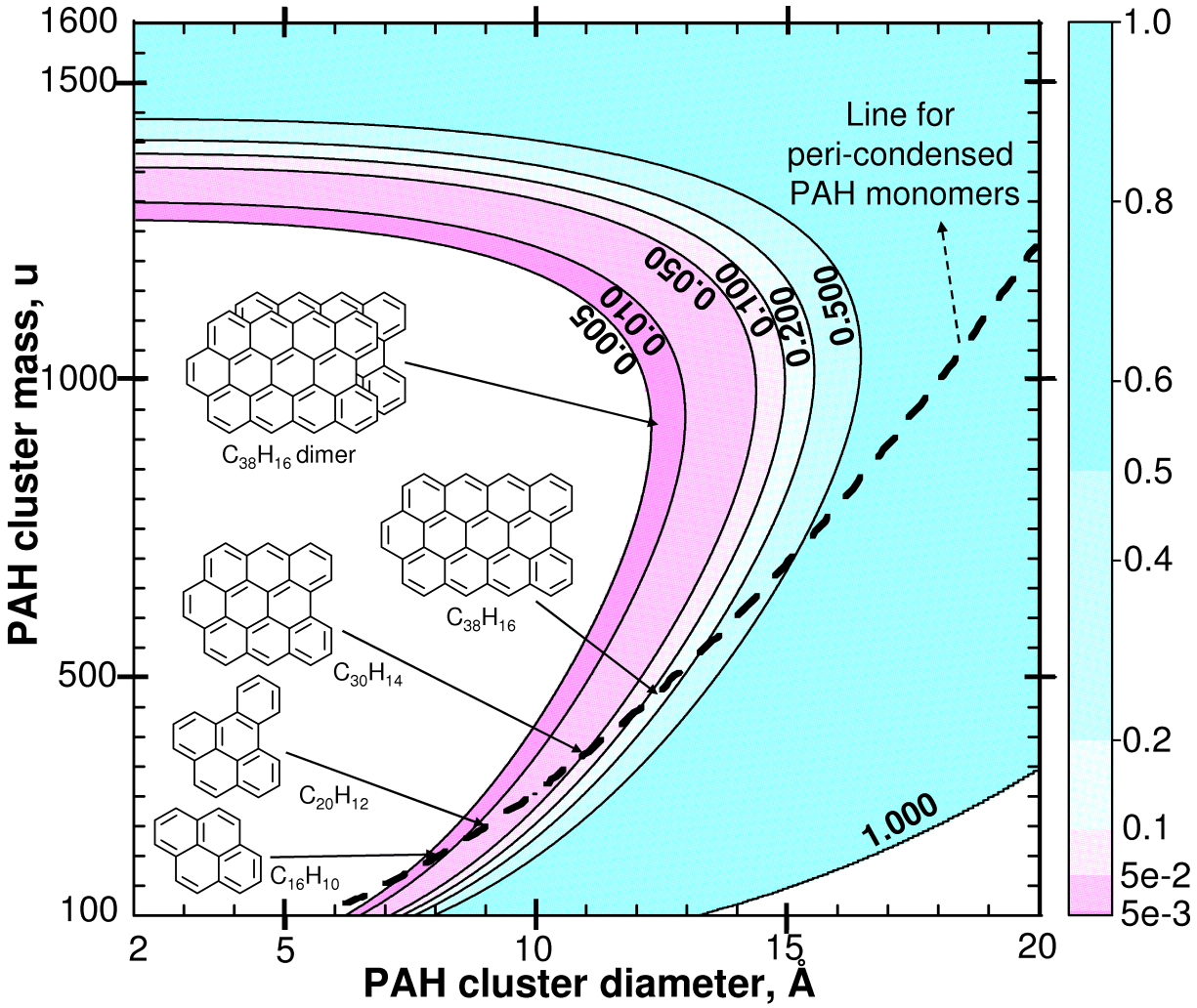

Figure 9: *A contour plot for the PAH collision efficiency* $C_{\rm E}$. *PAH coagulation starts taking place when the mass and collision diameter of the smaller of the two colliding PAH clusters become greater than 360 u and 10 Å, respectively (for example,* $\rm C_{30}H_{14}$*), when* $C_{\rm E} \geq 0.04$. *The dashed line in the figure represents the line for peri-condensed PAHs. The area above this line in the figure is only accessible to PAH clusters with more than one constituent PAHs (for example, a* $\rm C_{38}H_{16}$ *dimer).*

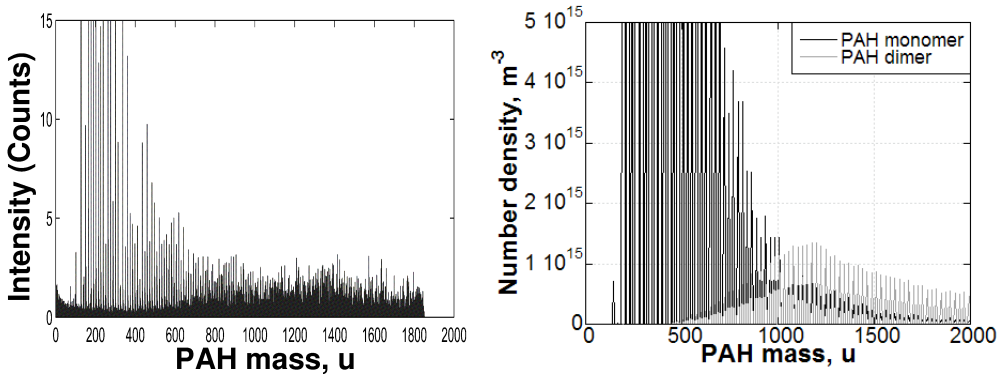

(a) Experimental mass spectra (b) Computed mass spectra

Figure 10: *PAH mass spectra at an operating pressure of 80 mbar (flame 1) at HAB = 30 mm. PAH monomers are represented by black lines, and dimers by grey lines in the computed spectra. At low pressure, the spectra for PAH dimers were widely spread over the PAH mass.*

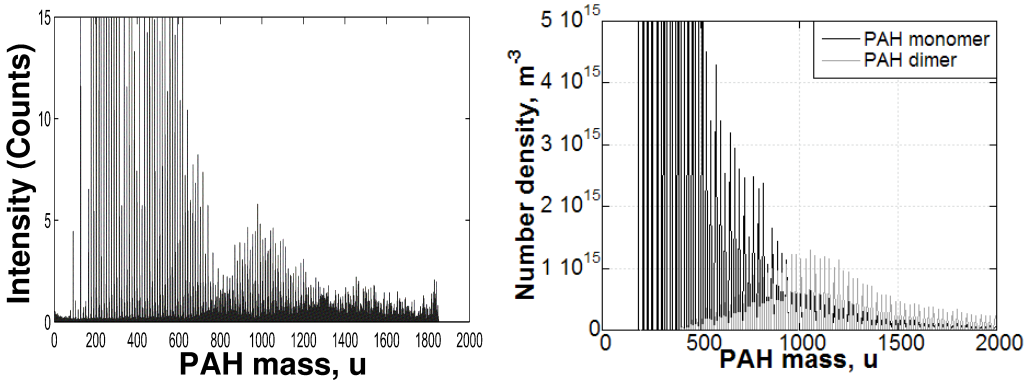

(a) Experimental mass spectra (b) Computed mass spectra

Figure 11: *PAH mass spectra at an operating pressure of 150 mbar (flame 3) at HAB = 30 mm. PAH monomers are represented by black lines, and dimers by grey lines in the computed spectra. At high pressures ($\geq$ 150), the computed spectra for PAH dimers were observed to shrink (narrow distribution over the PAH mass).*

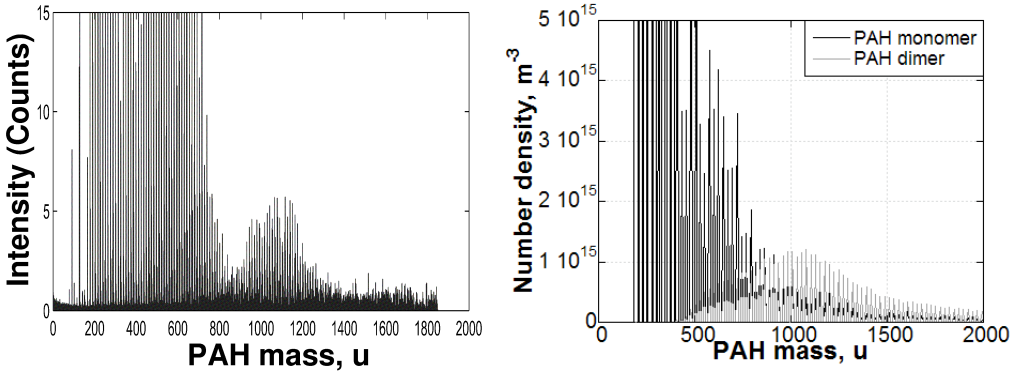

(a) Experimental mass spectra (b) Computed mass spectra

Figure 12: *PAH mass spectra at an operating pressure of 180 mbar (flame 4) at HAB = 30 mm. PAH monomers are represented by black lines, and dimers by grey lines in the computed spectra. At high pressures ($\geq$ 150), the computed spectra for PAH dimers were observed to shrink (narrow distribution over the PAH mass).*

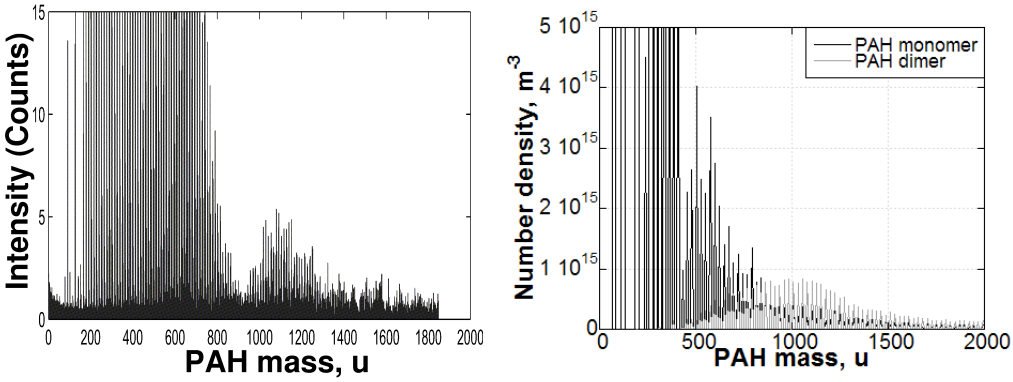

(a) Experimental mass spectra (b) Computed mass spectra

Figure 13: *PAH mass spectra at an operating pressure of 220 mbar (flame 5) at HAB = 30 mm. PAH monomers are represented by black lines, and dimers by grey lines in the computed spectra. At high pressures ($\geq$ 150), the computed spectra for PAH dimers were observed to shrink (narrow distribution over the PAH mass).*

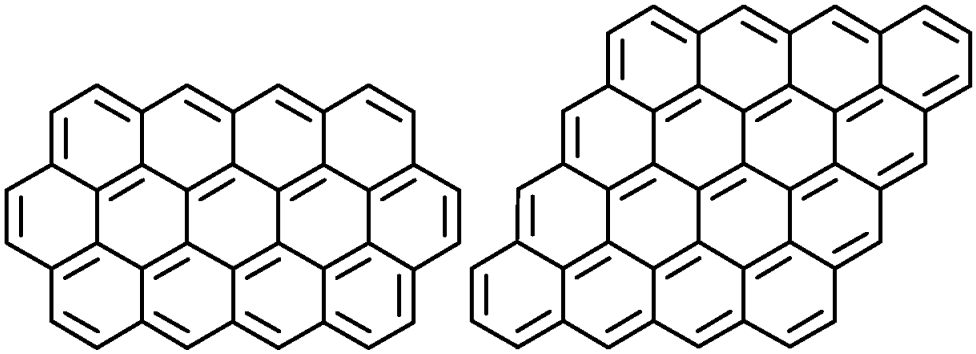

Figure 14: *Example computed PAHs ($C_{40}H_{16}$ and $C_{48}H_{18}$) present in a PAH dimer in flame 2 at HAB = 30 mm. The collision diameters of the two PAHs are 12.5 Å and 13.7 Å, and their masses are 496 u and 584 u, respectively. The collision efficiency for this PAH pair is 0.13.*

quicker conversion of PAH dimers to higher order stacks. This is evident from figure 15, as explained previously. Secondly, the number density of monomers with mass more than 1000 u were found to decrease with increasing pressure due to the reason explained above. Therefore, the mass spectra for PAH monomers and dimers shrank with increasing pressure. Thirdly, the maxima in the number density of computed PAH dimers were always obtained in the mass range of 1000 u to 1200 u, which is very close the experimental mass range of 900 u to 1150 u.

For high pressure flames, the computed spectra for monomers and dimers were found to be broader than the observed spectra. There can be two probable reasons behind it. Firstly, the assumption of equal accessibility of all the reactive sites on the PAHs in the KMC-ARS model leads to the formation of some large PAHs (with mass greater than 1000 u), which may not be present in flames. These large PAHs in the ensemble, though very low in concentration, can give rise to dimers of higher masses, leading to the broadening of the mass spectra of monomers and dimers. This shortcoming in the model is currently unavoidable. Secondly, the gas-phase chemical mechanism at 120 mbar pressure was used for all the flames, due to the absence of mechanisms at other pressures in the range of 80 – 220 mbar. This can also be responsible for the discrepancies between the observed and the computed spectra.

It is important to mention that the proposed correlation does not account for the change in C_E with flame parameters such as temperature. C_E can be a strong function of temperature, as a dimer which is not stable at flame temperature ($\approx$ 1800 K) may be stable at room temperature [3, 11, 17, 35]. Such a variation could not be captured with the available experimental data on PAH clusters, as the maximum flame temperatures varied within 50 K for all the flames (see figure 3). Therefore, the correlation in its present form is suitable for high temperature environments only. Further investigation, both experimental and theoretical, is required for a multi-dimensional treatment of collision efficiency, which can account for all the affecting parameters.

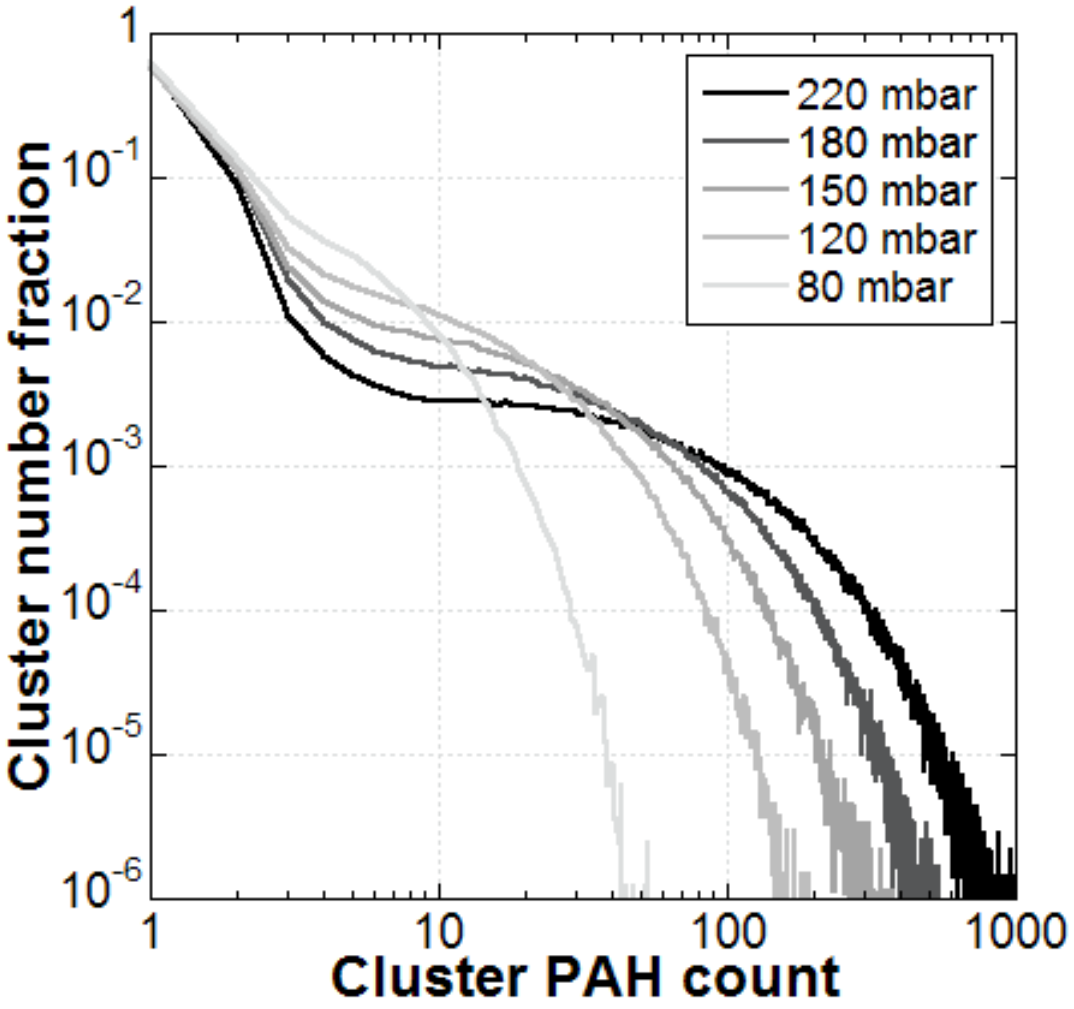

Figure 15: *Number fraction of the clusters with different numbers of PAHs comprising them, computed at different pressures (flames 1–5). A bimodality in the distribution of cluster number fraction is observed at higher pressures.*

6 Conclusion

This paper presents a study on the coagulation of PAH clusters in premixed laminar ethylene flame environments. A new multivariate PAH population balance model, named as the PAH-PP model was developed to simulate the coagulation of PAHs generated computationally using the previously developed PAH growth model, the KMC-ARS model. Both the models were solved using kinetic Monte Carlo methods. With the use of the PAH-PP model, the mass spectra of PAHs were generated computationally, and compared to the experimentally observed spectra. It was concluded that the collision efficiency of PAHs is an important parameter, which significantly affects the position of the maxima for PAH dimers and higher order stacks, and their spread in the computed spectra. To determine the factors on which the collision efficiency may depend, its variation with flame temperature, collision diameter, and mass of the colliding PAHs was studied. The collision efficiency was found to depend strongly on the mass and collision diameter of the smaller of the two colliding PAH clusters. By comparing the computed mass spectra with the experimental spectra for a C_2H_4-O_2 flame, a correlation for this efficiency, C_E was proposed. The same correlation was then used to generate the spectra for a number of premixed laminar C_2H_4-O_2 flames at different pressures. The position of the maxima of PAH dimers was very well predicted with the proposed correlation for all the flames. For two colliding PAHs, a very low value of collision efficiency was required to properly predict the position of the maxima of PAH dimers in the spectra, if one of them had mass less than 360 u and diameter less than 10 Å. This indicates that the collisions involving PAHs smaller than pyrene, or collisions between very large PAHs and small ones may not be successful in a high-temperature environment.

Acknowledgement

A.R. is grateful to Cambridge Commonwealth Trusts (CCT) and Clare College, Cambridge for their financial support. M.S. and M.K. acknowledge Churchill College for funding. The authors acknowledge the support of EPSRC under EP/C547241/1 and EP/E01724X/1.

References

[1] M. Alfè, B. Apicella, R. Barbella, J. N. Rouzaud, A. Tregrossi, and A. Ciajolo. Structure-property relationship in nanostructures of young and mature soot in premixed flames. *Proc. Combust. Inst.*, 32:697–704, 2009.

[2] J. Appel, H. Bockhorn, and M. Frenklach. Kinetic modeling of soot formation with detailed chemistry and physics: Laminar premixed flames of C_2 hydrocarbons. *Combust. Flame*, 121:122–136, 2000. doi:10.1016/S0010-2180(99)00135-2.

[3] J. Appel, H. Bockhorn, and M. Wulkow. A detailed numerical study of the evolution of soot particle size distributions in laminar premixed flames. *Chemosphere*, 42: 635–645, 2001. doi:10.1016/S0045-6535(00)00237-X.

[4] M. S. Celnik, R. I. A. Patterson, M. Kraft, and W. Wagner. Coupling a stochastic soot population balance to gas-phase chemistry using operator splitting. *Combust. Flame*, 148(3):158–176, 2007. doi:10.1016/j.combustflame.2006.10.007.

[5] M. S. Celnik, A. Raj, R. H. West, R. I. A. Patterson, and M. Kraft. An aromatic site description of soot particles. *Combust. Flame*, 155(1-2):161–180, 2008. doi:doi:10.1016/j.combustflame.2008.04.011.

[6] H. X. Chen and R. A. Dobbins. Crystallogenesis of Particles Formed in Hydrocarbon Combustion. *Combust. Sci. Technol.*, 159:109–128, 2000.

[7] A. D'Alessio, A. C. Barone, R. Cau, A. D'Anna, and P. Minutolo. Surface deposition and coagulation efficiency of combustion generated nanoparticles in the size range from 1 to 10 nm. *Proc. Combust. Inst.*, 30:2595–2603, 2005.

[8] A. D'Anna and J. H. Kent. A model of particulate and species formation applied to laminar non-premixed flames for three aliphatic-hydrocarbon fuels. *Combust. Flame*, 152:573–587, 2008.

[9] M. D. Domenico, P. Gerlinger, and M. Aigner. Detailed Soot Formation Model in Flames. In *European Combustion Meeting, Louvain-la-Neuve, Belgien*, 2005. URL `http://elib.dlr.de/3417`.

[10] A. Eibeck and W. Wagner. An efficient stochastic algorithm for studying coagulation dynamics and gelation phenomena. *SIAM J. Sci. Comput.*, 22(3):802–821, 2000. doi:10.1137/S1064827599353488.

[11] S. L. Fiedler, S. Izvekov, and A. Violi. The effect of temperature on nanoparticle clustering. *Carbon*, 45:1786–1794, 2007.

[12] M. Frenklach and H. Wang. Detailed modeling of soot particle nucleation and growth. *Proc. Combust. Inst.*, 23:1559–1566, 1990. doi:10.1016/S0082-0784(06)80426-1.

[13] M. Frenklach and H. Wang. Detailed surface and gas-phase chemical kinetics of diamond deposition. *Phys. Rev. B*, 43(2):1520–1545, 1991. doi:10.1103/PhysRevB.43.1520.

[14] M. Frenklach and H. Wang. *Detailed Mechanism and Modelling of Soot Particle Formation*, volume 59 of *Series in Chemical Physics*, pages 162–190. Springer Verlag, Berlin, 1994. ISBN 354058398X 9783540583981.

[15] M. Frenklach, C. A. Schuetz, and J. Ping. Migration mechanism of aromatic-edge growth. *Proc. Combust. Inst.*, 30:1389–1396, 2005. doi:10.1016/j.proci.2004.07.048.

[16] J. Happold. *Geschichtete polyzyklische aromatische Kohlenwasserstoffe als Bausteine der Rußbildung*. PhD thesis, Universität Stuttgart, 2008.

[17] J. Happold, H.-H. Grotheer, and M. Aigner. *Soot precursors consisting of stacked pericondensed PAHs*, pages 275–285. Proceedings of an International Workshop held in Villa Orlandi, Anacapri, May 13-16, 2007. Editor: H Bockhorn, A D'Anna, A F Sarofim and H Wang. Karlsruhe University Press.

[18] J. Happold, H.-H. Grotheer, and M. Aigner. Distinction of gaseous soot precursor molecules and soot precursor particles through photoionization mass spectroscopy. *Rapid Commun. Mass Sp.*, 21:1247–1254, 2007. doi:10.1002/rcm.2955.

[19] S. J. Harris and I. M. Kennedy. The coagulation of soot particles with Van-der-Waals forces. *Combust. Sci. Tech.*, 59(4):443–454, 1988. doi:10.1080/00102208808947110.

[20] J. D. Herdman and J. H. Miller. Intermolecular Potential Calculations for Polynuclear Aromatic Hydrocarbon Clusters. *J. Phys. Chem. A*, 112:6249–6256, 2008.

[21] K. H. Homann. Fullerenes and Soot Formation–New Pathways to Large Particles in Flames. *Angew. Chem.*, 37:2434–2451, 1998.

[22] T. Ishiguro, Y. Takatori, and K. Akihama. Microstructure of Diesel Soot Particles Probed by Electron Microscopy: First Observation of Inner Core and Outer Shell. *Combust. Flame*, 108:231–234, 1997. doi:10.1016/S0010-2180(96)00206-4.

[23] J. Kee, K. Grcar, M. D. Smooke, and J. A. Miller. PREMIX: A FORTRAN program for modelling steady laminar one-dimensional premixed flames. Technical report, SANDIA National Laboratories, 1985.

[24] R. J. Kee, F. M. Ropley, E. Meeks, and J. A. Miller. CHEMKIN-III: A FORTRAN chemical kinetics package for the analysis of gas-phase chemical and plasma kinetics. Technical Report UC-405 SAND96-8216, Sandia National Laboratories, Livermore, CA 94551-0969, USA, May 1996.

[25] B. Kumfer and I. Kennedy. *The role of soot in the health effects of inhaled airborne particles*, pages 1–15. Proceedings of an International Workshop held in Villa Orlandi, Anacapri, May 13-16, 2007. Editor: H Bockhorn, A D'Anna, A F Sarofim and H Wang. Karlsruhe University Press.

[26] J. T. Mckinnon and J. B. Howard. The roles of PAH and acetylene in soot nucleation and growth. *Proc. Combust. Inst.*, 24:965–971, 1992.

[27] J. H. Miller. The kinetics of polynuclear aromatic hydrocarbon agglomeration in flames. *Proc. Combust. Inst.*, 23:91–98, 1990. doi:10.1016/S0082-0784(06)80246-8.

[28] J. H. Miller. Aromatic excimers: evidence for polynuclear aromatic hydrocarbon condensation in flames. *Proc. Combust. Inst.*, 30:1381–1388, 2005.

[29] J. H. Miller, K. C. Smyth, and W. G. Mallard. Calculations of the dimerization of aromatic hydrocarbons: Implications for soot formation. *Proc. Combust. Inst.*, 20: 1139–1147, 1984.

[30] N. Morgan, M. Kraft, M. Balthasar, D. Wong, M. Frenklach, and P. Mitchell. Numerical simulations of soot aggregation in premixed laminar flames. *Proc. Combust. Inst.*, 31:693–700, 2007. doi:10.1016/j.proci.2006.08.021.

[31] R. I. A. Patterson, J. Singh, M. Balthasar, M. Kraft, and W. Wagner. Extending stochastic soot simulation to higher pressures. *Combust. Flame*, 145(3):638–642, 2006. doi:10.1016/j.combustflame.2006.02.005.

[32] A. Raj, M. Celnik, R. Shirley, M. Sander, R. Patterson, R. West, and M. Kraft. A statistical approach to develop a detailed soot growth model using PAH characteristics. *Combust. Flame*, 156:896–913, 2009. doi:10.1016/j.combustflame.2009.01.005.

[33] A. Raj, T. Totton, M. Sander, R. Shirley, M. S. Celnik, and M. Kraft. New PAH processes to improve the model prediction of the composition of combustion-generated PAHs and soot. Technical Report 69, c4e Preprint-Series, Cambridge, 2009. URL `http://como.cheng.cam.ac.uk`.

[34] M. Rapacioli, F. Calvo, F. Spiegelman, C. Joblin, and D. J. Wales. Stacked Clusters of Polycyclic Aromatic Hydrocarbon Molecules. *J. Phys. Chem. A*, 109:2487–2497, 2005. doi:10.1021/jp046745z.

[35] C. A. Schuetz and M. Frenklach. Nucleation of soot: Molecular dynamics simulations of pyrene dimerization. *Proc. Combust. Inst.*, 29:2307–2314, 2002.

[36] J. Singh, R. I. A. Patterson, M. Balthasar, M. Kraft, and W. Wagner. Modelling soot particle size distribution: Dynamics of pressure regimes. Technical Report 25, c4e Preprint-Series, Cambridge, 2004. URL `http://como.cheng.cam.ac.uk`. Material from this preprint has been published in Patterson et al. [31].

[37] J. Singh, M. Balthasar, M. Kraft, and W. Wagner. Stochastic modelling of soot particle size and age distribution in laminar premixed flames. *Proc. Combust. Inst.*, 30:1457–1465, 2005. doi:10.1016/j.proci.2004.08.120.

[38] J. Singh, R. I. A. Patterson, M. Kraft, and H. Wang. Numerical simulation and sensitivity analysis of detailed soot particle size distribution in laminar premixed ethylene flames. *Combust. Flame*, 145:117–127, 2006. doi:10.1016/j.combustflame.2005.11.003.

[39] R. L. Vander Wal. A TEM Methodology for the Study of Soot Particle Structure. *Combust. Sci. Tech.*, 126:333–357, 1997.

[40] R. L. Vander Wal. An Illustration of Soot Structure by Dark Field Transmission Electron Microscopy. *Combust. Sci. Tech.*, 132:315–323, 1998.

[41] R. L. Vander Wal and A. J. Tomasek. Soot nanostructure: dependence upon synthesis conditions. *Combust. Flame*, 136:129–140, 2004. doi:10.1016/j.combustflame.2003.09.008.

[42] R. L. Vander Wal, A. Yezerets, N. W. Currier, D. H. Kim, and C. M. Wang. HRTEM Study of diesel soot collected from diesel particulate filters. *Carbon*, 45:70–77, 2007. doi:10.1016/j.carbon.2006.08.005.

[43] A. Violi. Modeling of soot particle inception in aromatic and aliphatic premixed flames. *Combust. Flame*, 139:279–287, 2004. doi:10.1016/j.combustflame.2004.08.013.

[44] H. Wang and M. Frenklach. Calculations of rate coefficients for the chemically activated reactions of acetylene with vinylic and aromatic radicals. *J. Phys. Chem.*, 98(44):11465–11489, 1994. doi:10.1021/j100095a033.

[45] H. Wang and M. Frenklach. A detailed kinetic modeling study of aromatic formation in laminar premixed acetylene and ethylene flames. *Combust. Flame*, 110:173–221, 1997. doi:10.1016/S0010-2180(97)00068-0.